9

Research Article

Khaled Althubeiti*

Synthesis and characterization of the Co(II), Ni(II), and Cu(II) complexes with a 1,2,4-triazine derivative ligand

https://doi.org/10.1515/chem-2025-0186 received February 25, 2025; accepted July 6, 2025

Abstract: This study focuses on synthesizing a 1,2,4-triazine derivative, 5-(5-bromo-2-hydroxybenzylidene)-6-oxo-3-phenyl-5,6-dihydro-1,2,4-triazine-2(1H)-carbothio-amide (termed as HL), and the subsequent use of this ligand to capture three metal ions: Co(II), Ni(II), and Cu(II). The objectives included the synthesis of the ligand from 5-bromosalicylaldehyde and hippuric acid; the preparation of its metal complexes with the three transition metal ions; the verification of complexation stoichiometry using CHN and gravimetric analysis; the characterization of the ligand and complexes via spectroscopic techniques; the determination and comparison of their thermal properties through thermogravimetric (DTG) measurements; and the examination and comparison of their microstructures using powder X-ray diffraction (XRD) and transmission electron microscopy (TEM). Spectral, elemental, conductivity, and thermal data suggest general compositions of [CoL(H₂O)₄]-Cl·6H₂O for the Co(II) complex, [NiL(H₂O)₄]·Cl·4H₂O for the Ni(II) complex, and [CuL(H₂O)Cl]·2H₂O for the Cu(II) complex. TEM images revealed that the initially rod-like morphology of the ligand particles transformed into a stone-like appearance upon coordination with the Co(II), Ni(II), and Cu(II) ions. Finally, the antibacterial activity of the synthesized complexes was evaluated against five microbial strains to assess the impact of complexation on the antibacterial profile of the free ligand. The screening data indicated that the complexes exhibited improved antibacterial potency compared to the free ligand.

Keywords: 1,2,4-triazine derivative, metal ions, spectroscopic analyses, electron microscopy, antibacterial activity

1 Introduction

The chemical reactions between metallic elements and specialized molecules generate intriguing compounds known as metal-based complexes. These metal-based complexes are formed by coordinating the metallic element with the ligand through covalent bonds. The interaction between the metal and the ligand follows a donor-acceptor mechanism, where the ligand, acting as a Lewis base, donates electron pairs to the metal, while the metal, functioning as a Lewis acid, accepts these electron pairs. The ligand is an electron-rich molecule, which can be either inorganic or organic, possessing one or more pairs of electrons available for sharing with the metal. The number of donating atoms in the ligand is used to classify the ligands as monodentate, bidentate, tridentate, or polydentate [1–3]. Metal-based complexes exhibit unique properties, such as electrochemical, electronic, and spectroscopic characteristics, enabling them to have diverse applications ranging from physical and chemical sciences to biological and material applications. These metal-based complexes are used in various biological and industrial settings, including catalysis, ceramics, colors, dyes, nuclear fuels, and medical applications. The remarkable physicochemical properties of metal-based complexes, including redox activity, metal-ligand interactions, and coordination chemistry, allow researchers to optimize their effectiveness for therapeutic purposes. This includes adjusting the selectivity, stability, and lipophilicity of metal-based complexes to enhance their anticancer activity and minimize side effects. The use of these complexes as anticancer agents has been extensively explored and demonstrated over the years, and they continue to be the subject of ongoing research and development, with the goal of improving their efficacy and safety for the treatment of various types of cancers [4–7].

Transition metal complexes have garnered substantial scientific interest due to their diverse coordination geometries, oxidation states, and electronic configurations. These

^{*} Corresponding author: Khaled Althubeiti, Department of Chemistry, College of Science, Taif University, P.O. Box 11099, Taif, 21944, Saudi Arabia, e-mail: k.Althubeiti@tu.edu.sa

unique features have enabled the development of innovative catalysts, sensors, imaging agents, and therapeutic agents that have significantly advanced various fields. Transition metal complexes have a wide range of applications, from drug design to catalysis, playing a crucial role in the creation of therapeutic drugs, diagnostic tools, catalysts, functional materials, and medical imaging tools. They offer versatile solutions for diagnosing and treating various diseases, and their inherent redox properties make them ideal candidates for catalytic applications [8–10]. These complexes are recognized as valuable therapeutic and diagnostic agents, propelling advancements in inorganic medicinal chemistry. Transition metal-based complexes have been utilized to treat conditions such as cancer, neurological diseases, diarrhea, infections, and diabetes, and they exhibit beneficial biological activities, including antimicrobial, anti-inflammatory, and anti-tumor effects, making them invaluable in the pharmaceutical industry [6,11-14].

Nitrogen-containing heterocyclic compounds exhibit luminescence properties, such as photoluminescence and electroluminescence. Triazines, highly effective electronaccepting organic compounds, have been employed as electron transport layers in organic light-emitting diode devices. These triazines represent another class of nitrogen-containing heterocycles that have been extensively investigated for their unique photophysical and electrochemical characteristics. Versatile triazene synthons have found applications in various areas of organic synthesis, including pharmacology, total synthesis, polymer technology, and the construction of novel ring systems [15]. Fused 1,2,4-triazine aromatic rings are fundamental organic materials for optoelectronic applications. Furthermore, modifying triazine rings with various substituents at different positions holds great potential for developing new organic devices. This potential arises from the ability to fine-tune the electronic and optical properties of the triazine core through careful selection of substituents, enabling the creation of diverse organic materials for a range of optoelectronic applications, including organic light-emitting diodes, organic photovoltaics, and organic field-effect transistors. One approach to designing new triazine-based organic materials involves incorporating electron-donating units, such as aromatic amines, to generate push-pull systems [16].

This study specifically focuses on the synthesis of a 1,2,4-triazine derivative, namely 5-(5-bromo-2-hydroxybenzylidene)-6-oxo-3-phenyl-5,6-dihydro-1,2,4-triazine-2(1H)-carbothioamide (termed as HL), and the use of the synthesized ligand to capture three metal ions: Co(II), Ni(II), and Cu(II). The objectives of the study were (i) to synthesize the ligand (HL) from the reaction of 5-bromosalicylaldehyde and hippuric acid; (ii) to synthesize metal complexes of the ligand with three transition metal ions: Co(II), Ni(II), and Cu(II) (iii) to

utilize CHN elemental analysis and gravimetric analysis to verify the complexation stoichiometry between the ligand and the investigated metal ions; (iv) to use several spectroscopic techniques to structurally characterize the free ligand and the synthesized complexes; (v) to obtain and differentiate the thermal properties of the synthesized complexes using thermogravimetric (TG) and differential thermogravimetric (DTG) measurements; (vi) to observe and differentiate the microstructures of the synthesized complexes using powder X-ray diffraction (XRD) and transmission electron microscopy (TEM); and (vii) to assess the *in vitro* antibacterial activity of the synthesized complexes against two strains of Gram-negative bacteria and three strains of Gram-positive bacteria.

2 Research methodology

2.1 Reagents used

A variety of metal chlorides, including copper chloride, nickel chloride, and cobalt chloride, were provided by Sigma-Aldrich Chemical Company, while the specific reagents employed to synthesize the ligand were provided by Merck Chemical Company. Both companies offered these chemicals at the highest analytical grade purity. The metal chlorides were copper(II) chloride (CuCl₂; 134.45 g/mol; purity 99%), nickel(II) chloride (NiCl₂; 129.60 g/mol; purity 98%), and cobalt(II) chloride (CoCl₂; 129.84 g/mol; purity ≥98%). Rigorous safety protocols were enforced throughout the experiments to protect the well-being of the research personnel. The metal chlorides, organic compounds, and solvents were handled with meticulous consideration for the safety and welfare of the investigators. This included the mandatory use of personal protective equipment such as gloves, respirators, and safety goggles to shield the experimenters during all stages of the study. Furthermore, adequate ventilation and containment procedures were also implemented to further safeguard the health and safety of the research team throughout the experiments.

2.2 Manufacturing of the 1,2,4-triazine derivative

The ligand employed in this study is a 1,2,4-triazine derivative with the IUPAC name 5-(5-bromo-2-hydroxybenzylidene)-6-oxo-3-phenyl-5,6-dihydro-1,2,4-triazine-2(1H)-carbothioamide. It was synthesized following a previously established protocol [17]. To prepare the ligand, 0.01 mol of

5-bromosalicylaldehyde and 0.01 mol of hippuric acid were fused for approximately 1 h in the presence of a few drops of piperidine. This generated a yellow solid product, which was recrystallized in ethanol to obtain the pure compound. Around 3.44 g of the pure product, equivalent to 0.01 mol, was dissolved in 25 mL of glacial acetic acid, and then about 0.01 mol of thiosemicarbazide was added. The mixture was refluxed on a hot plate at 60°C for 4 h. The resulting precipitate was filtered from the system and thoroughly washed with diethyl ether and methanol. The product was then recrystallized in ethanol to obtain the pure ligand in a crystal form. The ligand yielded 78% of the expected amount and had a melting point of 243–245°C, indicating high purity. The chemical structure of the synthesized ligand is shown in Figure 1.

2.3 Manufacturing of metal-based complexes

The complexes of the ligand with the metal ions Co(II), Ni(II), and Cu(II) were synthesized through a multi-step procedure. This involved dissolving the ligand and metal chlorides, combining the reagents, collecting the resulting precipitates, and filtering and purifying the synthesized complexes. First, 2 mmol of the ligand was dissolved in 25 mL of methanol solvent, while the two millimoles of metal chlorides were dissolved in 25 mL of deionized water. The dissolution process was carefully monitored, with gentle heat applied as needed to ensure complete dissolution of the reagents, reflecting the precision and care involved. Next, the Co-L, Ni-L, and Cu-L mixed solutions were prepared by combining the methanolic ligand solution with the corresponding aqueous metal chloride solution. The beakers containing the mixtures were then placed on a hot plate with a magnetic stirrer. The chemical

Figure 1: Chemical structure of the synthesized ligand.

reaction between the ligand and each metal ion was allowed to proceed for 25 min under continuous stirring, with the pH of the reaction optimized at 8 using drops of 5% ammonium solution and the temperature set to 70°C. The precipitates of the Co–L, Ni–L, and Cu–L complexes were collected by evaporating the solutions until their volume was reduced by half and then allowing the solutions to stand overnight to ensure complete precipitation. The final step involved filtering and purifying the synthesized complexes by carefully collecting and filtering the generated precipitates and thoroughly washing the products with hot deionized water and diethyl ether. The purified Co–L, Ni–L, and Cu–L products were then dried in an electronic oven at 80°C.

2.4 Characterization techniques

The dried and purified ligand, along with the manufactured Co-L, Ni-L, and Cu-L complexes, underwent extensive analysis using a comprehensive suite of analytical techniques. This in-depth examination provided a thorough understanding of the structural, compositional, morphological, and thermal characteristics of the ligand and complexes. The characterization process involved the use of various instruments, including a Cary 7000 Agilent Technologies UV-Vis Spectrophotometer for UV-Vis spectra, a Bruker ALPHA FT-IR Spectrometer for FT-IR spectra, a Bruker DRX-250 NMR spectrophotometer for ¹H and ¹³C NMR spectra, and a Bruker D8 Advance X-ray Diffractometer for XRD spectra. Thermal and elemental data were obtained using a Q500 V20.10 Build 36 Thermal Analyzer and a Perkin-Elmer 2400 series II CHNS elemental analyzer, respectively. Additionally, the detailed morphology of the synthesized complexes was observed using high-resolution TEM images captured using a JEM-2010 JEOL Microscope operated at an electron accelerating voltage of 200 kV.

2.5 Antibacterial activities

The antibacterial potency of the synthesized complexes was evaluated using a modified Kirby–Bauer disc diffusion technique [18–20]. Specifically, for each bacterium, a $100~\mu L$ aliquot of a fresh culture containing approximately 10^8 cells/mL was cultured in 10 mL of media. This microbial suspension was then spread onto agar plates. Representative colonies of each organism with potential pathogenic

characteristics were selected from primary agar plates and tested using the disc diffusion method to assess susceptibility [18–20]. Plates inoculated with Gram-positive bacteria, such as *Bacillus subtilis, Staphylococcus aureus*, and *Streptococcus pneumoniae*, as well as Gram-negative bacteria, including *Escherichia coli* and *Pseudomonas aeruginosa* were incubated at 35–37°C for 1–2 days. The diameters of the inhibition zones were measured in millimeters to quantify the antibacterial efficacy of the target complexes. Tetracycline discs served as positive controls, while filter discs impregnated with 10 μL of solvent were used as negative controls. The antibiotic discs were placed on the agar surface after the bacterial culture was spread and allowed to dry for 5–10 min; after which, the plates were incubated at 37°C for 24 h.

3 Results and discussion

3.1 Manufactured ligand

The investigated ligand in this study is a 1,2,4-triazine derivative with the IUPAC name 5-(5-bromo-2-hydroxybenzylidene)-6-oxo-3-phenyl-5,6-dihydro-1,2,4-triazine-2(1H)carbothioamide, which was synthesized using a previously described protocol [17]. The overall chemical reaction for the ligand's synthesis was provided in the Supplementary Data file. The synthesized ligand was subjected to identification and characterization using melting point analysis, elemental analysis, FT-IR, and ¹H and ¹³C NMR spectroscopy. The spectra are provided in the Supplementary Data file. The ¹H and ¹³C NMR spectra were recorded at room temperature using DMSO- d_6 as the solvent. The ligand demonstrated solubility in methanol, ethanol, and common organic solvents like DMF and DMSO, but was insoluble in diethyl ether, carbon tetrachloride, dichloromethane, and chloroform. The ligand's solubility profile suggests its potential for diverse applications in chemical and pharmaceutical formulations.

A sample of the manufactured ligand gives the following results: orange-colored powder; $C_{17}H_{13}BrN_4O_2S$ (417.28 g/mol); yield: 78%; CHN elemental data: observed (%): C 48.60; H 3.06; N 13.37; S, 7.66; Br, 19.10. IR bands (cm⁻¹): 3,414 v(O–H), 3,306 and 3,075 v(N–H) of the –NH2 group, 3,198 v(N–H) of the –NH group, 1,729 v(C=O), 1,645 $\delta_{sciss}(N-H)$, 1,527 v(C=N), 1,487 v(C=C), 1,451 $\delta(C-O-H)$, 1,351 v(C=S), 1,294 v(C-O), 1,220 $\nu_{asym}(C-N)$, 1,171 v(C-Br), 1,064 $\nu_{sym}(C-N)$, 1,027 v(C-C), 860 v(C=S), 689 v(O–H) outof-plane bending. The ¹H NMR chemical shifts (500 MHz, DMSO- d_6) were δ = 10.02 (s,1H, NH), 8.68 (s, 1H, OH), 7.89 (m,

2H, $C_{3,5}H$), 7.88 (s, 1H, $C_{3}H$), 7.60 (t, 1H, J = 13.5 Hz, $C_{4}H$), 7.55 (t, 2H, J = 10.0 Hz, $C_{1,6}H$), 7.52 (d, 1H, J = 7.5 Hz, $C_{5}H$), 7.39 (d, 1H, J = 8.5 Hz, $C_{6}H$), 7.22 (s, 2H, NH₂), 7.18 (s, 1H, CH=). The ¹³C NMR spectral assignments (125 MHz, DMSO- d_{6}) were δ = 181.2 (C=S), 167.2 (C=O), 160.5 C_{3} triazine, 142.5 C_{1} , 139.2 HC = C_{1} , 135.0 C_{5} , 132.7 HC = C, 129.0 C_{4} , 128.7 C_{3} , 127.0 C_{2} , 123.3 C_{6} , 117.5 C_{4} . Analyses of the synthesized ligand demonstrate that its experimentally determined CHN elemental data closely align with the theoretically calculated values (C 48.37%, H 3.20%, N 13.62%, S 7.90%, Br 18.95%) based on its molecular structure ($C_{17}H_{13}$ BrN₄O₂S; 417.28 g/mol).

3.2 Manufactured complexes

3.2.1 Compositions

The manufactured ligand was employed to capture Co(II), Ni(II), and Cu(II) ions from aqueous solutions. The ligand—metal complexes are referred to as Co–L, Ni–L, and Cu–L, respectively. After preparing and purifying the ligand—metal complexes, their elemental compositions, including the presence and number of carbon, hydrogen, nitrogen, sulfur, and metal atoms, were analyzed. The metal and water contents were determined using a gravimetric technique, while the contents of carbon, hydrogen, nitrogen, and sulfur were determined using a CHN elemental analyzer. The compositions of the synthesized complexes, including the quantities of carbon, hydrogen, nitrogen, sulfur, metal, and water, are described in detail below:

- (i) Complex Co–L: the complex has the chemical formula $C_{17}H_{32}BrN_4O_{12}SClCo$, with a molecular weight of 690.66 g/mol. The microanalytical data show the following percentages (%): found (calculated): C, 29.66 (29.54); H, 4.80 (4.63); N, 7.96 (8.11); S, 4.85 (4.63); Cl, 5.40 (5.13); Co, 8.36 (8.53); and H_2O , 26.91 (26.06).
- (ii) Complex Ni–L: the complex has the chemical formula $C_{17}H_{28}BrN_4O_{10}SClNi$, with a molecular weight of 654.42 g/mol. The microanalytical data show the following percentages (%): found (calculated): C, 31.31 (31.17); H, 4.52 (4.28); N, 8.45 (8.56); S, 4.73 (4.89); Cl, 5.65 (5.42); Ni, 8.74 (8.97); and H_2O , 22.19 (22.0).
- (iii) Complex Cu–L: the complex has the chemical formula $C_{17}H_{18}BrN_4O_5SClCu$, with a molecular weight of 569.28 g/mol. The microanalytical data shows the following percentages (%): found (calculated): C, 35.59 (35.83); H, 3.45 (3.16); N, 10.0 (9.84); S, 5.49 (5.62); Cl, 6.08 (6.23); Cu, 11.30 (11.16); and H_2O , 9.72 (9.49).

The measured values for carbon, hydrogen, nitrogen, sulfur, chlorine, metals, and water match the calculated

DE GRUYTER Metal complexes of 1,2,4-triazine — 5

values, confirming the accuracy of the chemical analysis. The consistency between the measured and calculated data provides strong evidence supporting the reliability and precision of the analytical methods used. The compositions of the ligand–metal complexes suggest a 1:1 reaction stoichiometry (ligand to metal), which aligns with the proposed general compositions of $[CoL(H_2O)_4]\cdot Cl\cdot 6H_2O$ for the ligand complex with Co(II), $[NiL(H_2O)_4]\cdot Cl\cdot 4H_2O$ for the ligand complex with Ni(II), and $[CuL(H_2O)Cl]\cdot 2H_2O$ for the ligand complex with Cu(II), respectively. The suggested chemical formulas $C_{17}H_{32}BrN_4O_{12}SClCo$, $C_{17}H_{28}BrN_4O_{10}SClNi$, and $C_{17}H_{18}BrN_4O_5SClCu$ represent the corresponding Co-L, Ni-L, and Cu-L complexes.

3.2.2 UV-Visible spectroscopy and conductivity measurements

DMSO solutions containing the uncoordinated ligand, the Co–L complex, the Ni–L complex, and the Cu–L complex were analyzed using a UV-Vis spectrometer, and the resulting spectra are presented in Figure 2. The analysis of these solutions offered valuable insights into the spectral characteristics of the different ligand–metal complexes, which can be further explored to enhance our understanding of their structural and electronic properties. Table 1 lists the characteristic UV-Vis band wavelengths and their assigned transitions for the free ligand and its complexes. The UV-Vis spectrum of the uncoordinated ligand exhibits a broad range of absorption. It absorbs light wavelengths from 200 to 600 nm. Within this range, it displays a prominent absorption band at

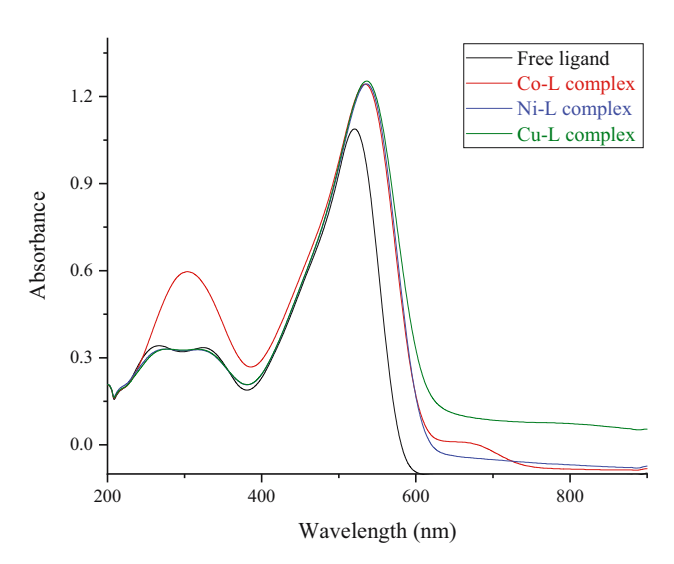


Figure 2: UV-Vis absorption profiles of the uncoordinated ligand and the ligand–metal complexes.

520 nm, as well as two medium-intensity twin bands at 268 and 324 nm. The strong 520 nm band is approximately three times more intense than the twin bands. The width of the intense 520 nm band is around 125 nm. The 520 nm band is likely attributed to $n \to \pi^*$ electronic transitions, which involve the promotion of an electron from a nonbonding orbital (n) to an anti-bonding π orbital. In contrast, the twin bands at 268 and 324 nm can be attributed to $\pi \to \pi^*$ electronic transitions, where an electron is promoted from a bonding π orbital to an anti-bonding π^* orbital. The ligand does not absorb any light beyond 600 nm. The UV-Vis spectrum of the uncoordinated ligand exhibits an enhanced intensity and broadening of the 520 nm band upon coordination with Co(II), Ni(II), and Cu(II) ions. Additionally, the band's maximum shifts from 520 nm in the uncoordinated ligand to 535 nm in the coordinated ligand. This observed shift in the band maximum and the broadening of the 520 nm band suggest a change in the electronic structure of the ligand upon coordination with the metal ions. The enhanced intensity of the 520 nm band may indicate an increase in the molar absorptivity of the ligand, potentially due to the formation of a more stable coordination complex. After coordination with the metal ions, the uncoordinated ligand's UV-Vis spectrum, which originally featured twin absorption bands at 268 and 324 nm, is now characterized by a single absorption band at 303 nm in the ligand complexes with Co(II), Ni(II), and Cu(II) ions. This bathochromic shift and simplification of the absorption spectrum suggest a change in the electronic structure of the ligand upon coordination with the metal centers.

Conductivity measurements offer valuable insights into the charge dynamics and ionization states of organic—metal compounds. In this study, we used a digital conductivity meter to measure the conductivity of the uncoordinated ligand and its metal complexes at room temperature. This approach allows us to elucidate the charge transfer

Table 1: Characteristic UV-Vis band wavelengths (λ_{max}) and their assigned transitions for the free ligand and its complexes

Compound	Band wavelengths (λ _{max}); nm	Assigned transitions
Free ligand	268, 324	$\pi \to \pi^*$
	520	$n \rightarrow \pi^*$
Co-L complex	303	$\pi \to \pi^*$
	535	$n \to \pi^{\textstyle *}$
Ni-L complex	303	$\pi \to \pi^*$
	535	$n \to \pi^{\textstyle *}$
Cu-L complex	303	$\pi \to \pi^*$
	535	$n \rightarrow \pi^*$

and electron delocalization within these systems, which is crucial for understanding their structural, electronic, and functional characteristics. We found that the molar conductance of the uncoordinated ligand in DMSO was 8.13 Am, confirming its non-conducting nature. In stark contrast, the molar conductance values of the Co-L, Ni-L, and Cu-L complexes in DMSO were 52.10, 61.05, and 30.28 Am, respectively. The significantly higher values for Co-L and Ni-L strongly indicate their electrolytic properties, which can be attributed to the presence of one chloride ion outside the coordination sphere of these complexes, facilitating ion mobility and thus higher conductivity. The molar conductance of the Cu-L complex, while lower than Co-L and Ni-L, still indicates a slightly electrolytic nature. This suggests that, although a chloride ion is within its coordination sphere, it can still dissociate and exist as a free ion in solution. This dissociation increases the solution's conductivity, explaining the relatively higher conductivity of the Cu-L complex compared to a neutral complex in DMSO.

3.2.3 FT-IR spectroscopy

Infrared spectroscopy is a powerful analytical technique that offers valuable insights into the coordination environment of ligands. This method reveals changes in the spectra of metal complexes, providing information about their structure and bonding. The synthesized ligand—metal complexes were analyzed using FT-IR spectroscopy, and the recorded spectra are included in the Supplementary Data file. The resulting IR spectral data (in cm⁻¹) obtained from their FT-IR analyses are as follows:

- (i) Complex Co–L: 3,300 and 3,077 ν (N–H) of the –NH₂ group, 3,198 ν (N–H) of the –NH group, 1,732 ν (C=O), 1,644 δ_{sciss} (N–H), 1,582 ν (C=N), 1,486 ν (C=C), 1,450 δ (C–O–H), 1,350 ν (C=S), 1,294 ν (C–O), 1,223 ν_{asym} (C–N), 1,171 ν (C–Br), 1,065 ν_{sym} (C–N), 1,018 ν (C–C), 868 ν (C=S), 690 ν (O–H) out-of-plane bending, 545 ν (M–O), 497 ν (M–N).
- (ii) Complex Ni–L: 3,310 and 3,080 ν (N–H) of the –NH₂ group, 3,200 ν (N–H) of the –NH group, 1,731 ν (C=O), 1,644 δ_{sciss} (N–H), 1,585 ν (C=N), 1,487 ν (C=C), 1,450 δ (C–O–H), 1,349 ν (C=S), 1,294 ν (C–O), 1,222 ν_{asym} (C–N), 1,172 ν (C–Br), 1,065 ν_{sym} (C–N), 1,018 ν (C–C), 860 ν (C=S), 690 ν (O–H) out-of-plane bending, 548 ν (M–O), 495 ν (M–N).
- (iii) Complex Cu–L: 3,308 and 3,074 ν (N–H) of –NH₂ group, 3,199 ν (N–H) of –NH group, 1,726 ν (C=O), 1,644 δ_{sciss} (N–H), 1,580 ν (C=N), 1,487 ν (C=C), 1,451 δ (C–O–H), 1,356 ν (C=S), 1,294 ν (C–O), 1,224 ν_{asym} (C–N), 1,172

 ν (C–Br), 1,065 ν _{sym}(C–N), 1,018 ν (C–C), 858 ν (C=S), 691 ν (O–H) out-of-plane bending, 553 ν (M–O), 498 ν (M–N).

FT-IR spectral analysis of the uncoordinated ligand and its corresponding ligand-metal complexes shows significant changes in the frequency and intensity of various characteristic bands. These observed shifts can be directly attributed to the anticipated modifications in the symmetry and electronic structure of the ligand upon complexation, in comparison to the uncoordinated state. The uncoordinated ligand consists of six functional groups: -OH, -NH₂, -NH, C=O, C=N, and C=S. The -OH group vibration produced a distinct and intense IR band at 3,414 cm⁻¹. The -NH₂ group vibration generated a distinct and intense IR band at 3,306 cm⁻¹ and a weaker band at 3,075 cm⁻¹. The –NH group exhibited a distinct and intense absorption band at 3,198 cm⁻¹. After the ligand coordinated with Co(II), Ni(II), and Cu(II) ions, the characteristic band of the ν (O–H) vibrational mode was no longer observed in the FT-IR spectra of the resulting ligand-metal complexes, indicating deprotonation. The formation of complexes between the ligand and the studied metal ions leads to the deprotonation of the ligand. This results in the disappearance of the characteristic IR band corresponding to the $\nu(O-H)$ vibrational mode of the hydroxyl functional group. The deprotonated hydroxyl group of the ligand participates in complexation with the Co(II), Ni(II), and Cu(II) ions, leading to the emergence of new and medium-intensity IR bands at 545, 548, and 553 cm⁻¹ for the Co-L, Ni-L, and Cu-L complexes, respectively, which originate from the ν (M–O) vibrations [21]. The interaction between the ligand and the studied metal ions had a negligible effect on the vibrational frequencies of the -NH₂, -NH, C=O, and C=S functional groups. Their frequencies were only slightly altered or remained largely unaffected in the ligand-metal complexes compared to the uncoordinated ligand. The band corresponding to the $\nu(C=N)$ vibrations exhibited significant shifts when the ligand formed complexes with the studied metal ions. This band was observed at 1,527 cm⁻¹ in the uncoordinated ligand, but it shifted to 1,582 cm⁻¹ in the Co-L complex, 1,585 cm⁻¹ in the Ni-L complex, and 1,580 cm⁻¹ in the Cu–L complex. The participation of the ligand's C=N bond in complexation with the Co(II), Ni(II), and Cu(II) ions led to the emergence of new and medium-intensity IR bands at 497, 495, and 498 cm⁻¹ for the Co-L, Ni-L, and Cu-L complexes, respectively, which could be attributed to the $\nu(M-N)$ vibrations, indicating that the ligand coordinated with the studied metal ions through the nitrogen lone pair electrons of the C=N group [22]. The acquired spectral, elemental, and conductivity data were employed to suggest appropriate chemical structures for the synthesized Co–L, Ni–L, and Cu–L complexes, as shown in Figure 3.

3.2.4 XRD reflections and TEM imaging

XRD and TEM analysis provided detailed information about the structural properties, phase purity, morphology, and particle characteristics of the synthesized ligandmetal complexes. The XRD reflections for the uncoordinated ligand and ligand-metal complexes were acquired at an accelerating voltage of 40 kV, a current of 30 mA, over an angular range of 5–70°, and a temperature of 25°C; the recorded XRD spectra are included in the Supplementary Data file. The XRD instrument utilized a Cu $K_{\alpha 1}$ source and a Ge monochromator. The XRD spectroscopic data presented in Table 2 highlight the most significant peaks for the uncoordinated ligand and the ligand-metal complexes, providing valuable insights into their crystalline structure and phase composition. The XRD analysis of the uncoordinated ligand revealed four distinct peaks: a very intense peak, a moderately strong peak, and two peaks of medium

Table 2: XRD spectroscopic data of the most prominent peaks for the uncoordinated ligand and the ligand–metal complexes

Compound	2θ (°)	Net height	FWHM (°)	<i>d-</i> spacing value (Å)
Free ligand	21.422	79.7	0.362	4.14461
	25.310	61.0	0.428	3.51609
	28.105	44.9	0.611	3.17237
	42.130	51.4	0.688	2.14315
Co-L	21.450	48.4	0.394	4.13928
Ni-L	21.759	77.4	0.454	4.08128
	33.077	41.8	0.492	2.70606
Cu-L	20.172	18.2	0.454	4.39847
	21.895	48.2	0.382	4.05605
	25.642	20.2	0.369	3.47133

intensity. The most prominent and strongest peak was observed at a Bragg angle 2θ of 21.4222°. Additionally, a moderately strong peak was found at a Bragg angle 2θ of 25.310°. Furthermore, two medium-intensity diffraction peaks were detected at 2θ values of 28.105 and 42.130°. The Co–L complex demonstrated a single, extremely

Figure 3: Chemical structures proposed for synthesized ligand-metal complexes.

8 — Khaled Althubeiti DE GRUYTER

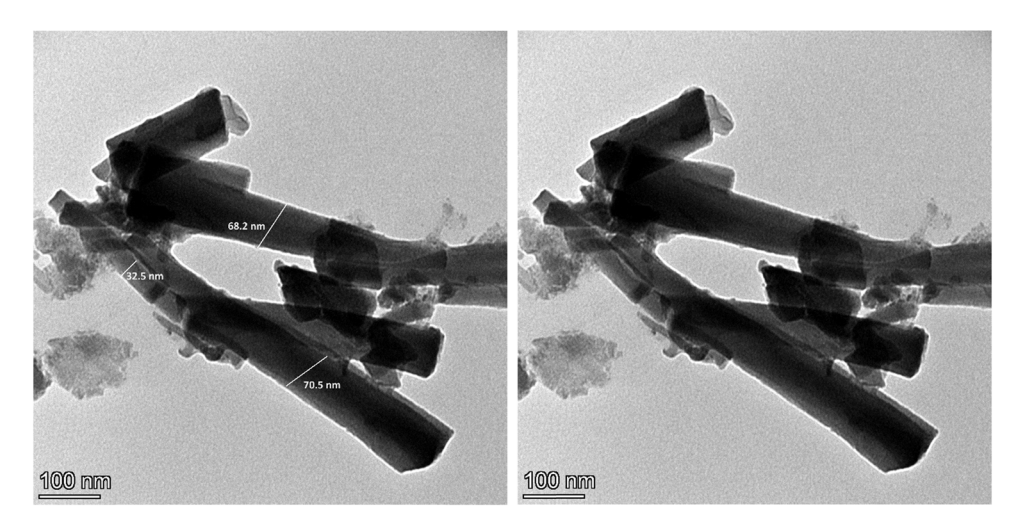


Figure 4: TEM images of the uncoordinated ligand.

intense diffraction peak at a Bragg angle 2θ of 21.450° . Additionally, the X-ray diffraction pattern of this complex exhibited ten supplementary low-intensity peaks. This X-ray diffraction profile of the Co–L complex indicates a highly crystalline structure with a regular and well-ordered arrangement of atoms or molecules within its frameworks, suggesting a highly organized and structured material. The XRD patterns of the Ni–L and Cu–L complexes showed two and three XRD reflections, respectively. The Ni–L complex exhibited a very strong diffraction peak at a Bragg angle 2θ of 21.759° , and a medium-intensity peak at a 2θ angle of 33.077° . Conversely, the Cu–L complex presented a most prominent and intense peak at a Bragg angle 2θ of 21.895° , along with two medium-intensity peaks at 2θ angles of 20.172° and 25.642° .

Micrographs obtained using transmission electron microscopy (TEM) offer comprehensive insights into the structural features, distributions, shapes, and particle dimensions of the materials, equipping researchers with a thorough understanding of their properties and potential applications. In this work, we employed a high-resolution microscope to visualize and explore the microstructural variations among the synthesized ligand—metal complexes, providing valuable information about their structural characteristics. The resulting images are shown in Figures 4–7, allowing for a detailed examination and analysis of the sample's morphology and composition. The high-quality and well-focused TEM images show that most of the uncoordinated ligand particles had an elongated, rod-like shape. The ligand rods varied significantly

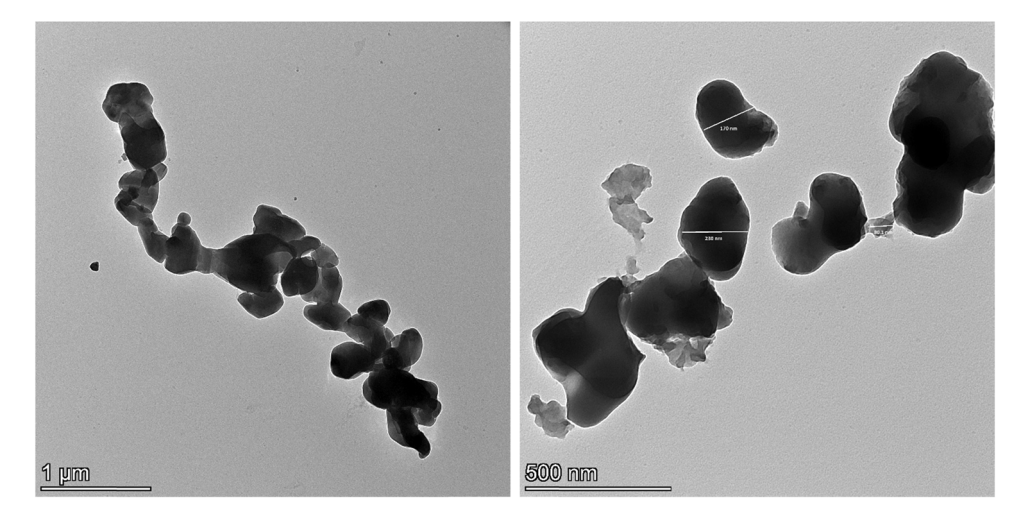


Figure 5: TEM images of the Co-L complex.

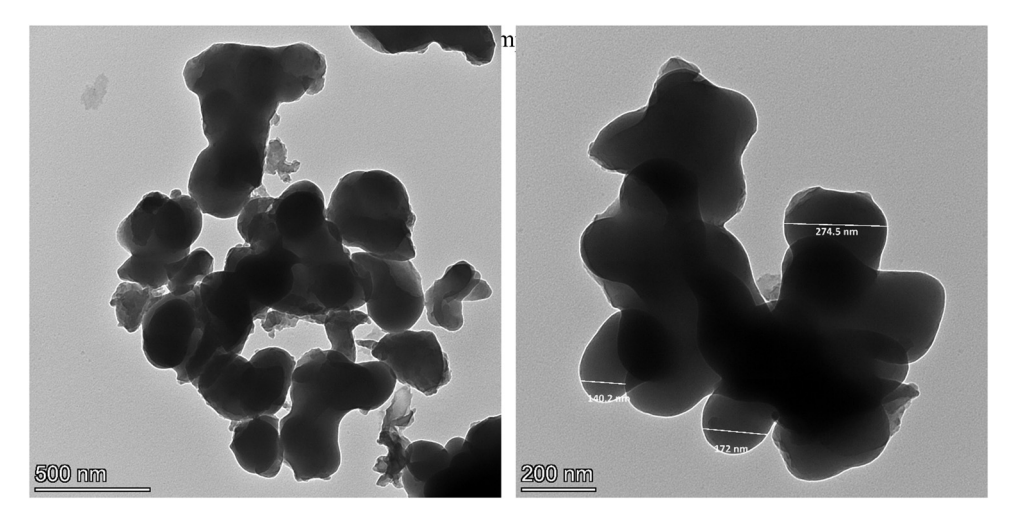


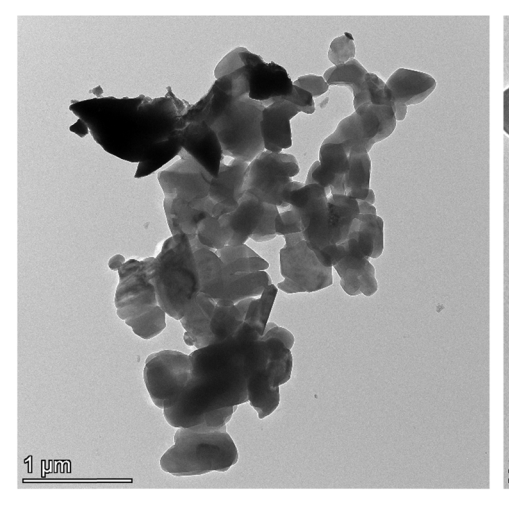
Figure 6: TEM images of the Ni-L complex.

in size and thickness, with an average length of approximately 300 nm and an average width of around 50 nm. Specifically, the rods ranged in length from around 200 nm to 400 nm, and their widths spanned a range of 40-60 nm. The coordination of the ligand with the Co, Ni, and Cu ions resulted in a transition from a rod-like to a more irregular, stone-like morphology of the particles. The resulting stone-like particles of the Co-L, Ni-L, and Cu-L complexes exhibited a range of shapes, sizes, and thicknesses, and these structures tended to group together, forming cluster-like arrangements. The differences in shapes, sizes, and thicknesses, as well as the cluster-like arrangement of these stone-like particles, could have resulted in a significantly increased surface area of the complexes, potentially enhancing their catalytic performance to a greater degree. The increased surface area

and unique morphology of the stone-like particles may have also contributed to other beneficial properties, such as improved adsorption capacity or enhanced mass transfer kinetics, which could further optimize the catalytic activity of the Co-L, Ni-L, and Cu-L complexes.

3.2.5 Examination of thermal patterns

Spectral, elemental, and conductivity data obtained were used to propose suitable chemical structures for the synthesized Co-L, Ni-L, and Cu-L complexes. These data suggest general compositions of [CoL(H₂O)₄]·Cl·6H₂O for the ligand complex with Co(II), [NiL(H₂O)₄]·Cl·4H₂O for the ligand complex with Ni(II), and [CuL(H2O)Cl]·2H2O. To further confirm the proposed compositions and structures



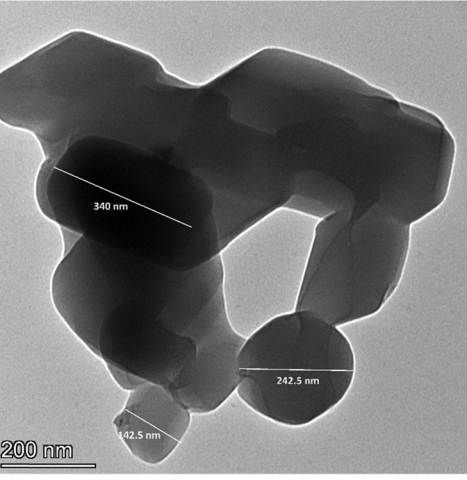


Figure 7: TEM images of the Cu-L complex.

Table 3: Thermal decom	position data of the	uncoordinated ligand and	the ligand-metal complexes

Compound	Stages	TG range (°C)	TG% mass loss		Lost species	
			Found	Calculated		
Free ligand	I	230–300	19.15	19.17	H ₂ S + NO ₂	
	II	300-700	80.68	80.74	$5C_2H_2 + HBr + 7CO_2 + 3NO_2$	
Co-L	I	200-350	31.20	31.34	10H ₂ O + HCl	
	II	350-800	49.05	49.10	$H_2S + 4NO_2 + HBr + 4C_2H_2 + 4CO_2$	
	Residue	_	19.28	19.53	CoO + 5C	
Ni-L	I	175-240	10.88	11.00	4H ₂ O	
	II	240-350	16.36	16.58	4H ₂ O + HCl	
	III	350-800	60.72	60.96	$H_2S + 4NO_2 + HBr + 4C_2H_2 + 9CO_2$	
	Residue	_	11.30	11.41	NiO	
Cu-L	I	150-200	9.35	9.46	3H ₂ O	
	II	200-300	12.18	12.38	H ₂ S + HCl	
	III	300-800	53.49	53.62	4NO ₂ + HBr + 4C ₂ H ₂ + 4CO ₂	
	Residue	_	24.40	24.51	CuO + 5C	

of the created ligand—metal complexes, the next step is to characterize them through thermogravimetric measurements. The thermal degradation patterns can provide additional support for the proposed compositions and structures of the synthesized ligand—metal complexes. This analysis can also offer valuable insights into the thermal stability and decomposition characteristics of these coordination compounds. Table 3 lists the expected thermal degradation patterns for the uncoordinated ligand and the ligand—metal complexes, derived from their thermograms shown in Figure 8. An examination of the products' thermograms revealed the following observations:

(i) A well-aligned trend emerged between the calculated and experimental results. This finding supports the

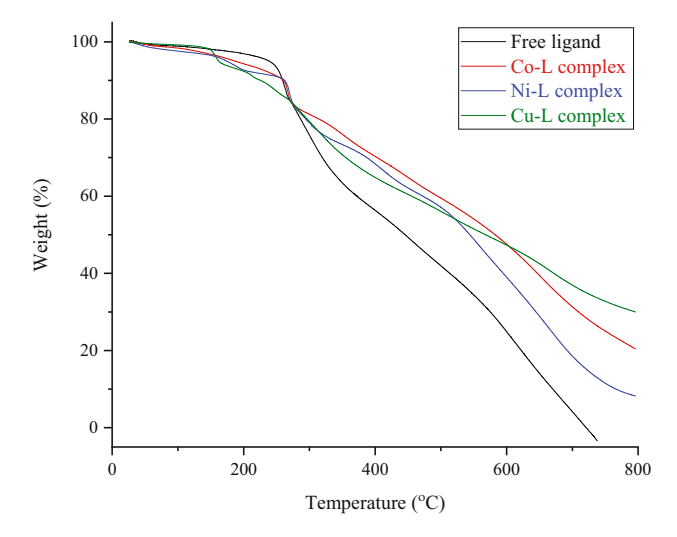


Figure 8: Thermograms of the uncoordinated ligand and the ligandmetal complexes.

- stoichiometry identified through empirical inquiry. The robust consistency between the calculated and experimental data offers compelling evidence that the stoichiometry accurately reflects the composition of the synthesized ligand—metal complexes.
- (ii) The free ligand demonstrated high thermal stability, withstanding temperatures up to 230°C without degradation. However, combining the ligand with Co(II), Ni (II), and Cu(II) ions significantly diminished its thermal stability, lowering it to below 200°C, likely due to the relatively weak ligand–metal bonds. Forming the ligand–metal bonds reduces the thermal endurance and mechanical durability of the free ligand. This implies that the ligand's structural strength and resistance to physical stress are weakened, rendering it more susceptible to thermal degradation and damage at lower temperatures compared to the uncombined ligand.
- (iii) The thermal stability of the uncoordinated ligand and its metal complexes showed a decreasing trend in the following order: free ligand > Co-L > Ni-L > Cu-L. This pattern is influenced by various factors, including the strength of the metal-ligand bond, the size and charge of the metal ion, as well as the specific coordination environment surrounding the metal center. These aspects all contribute to the observed differences in thermal stability.
- (iv) The complexes formed by the ligand and Ni(II) or Cu(II) ions underwent a three-step degradation process. Conversely, the Co–L complex exhibited a two-step degradation process.
- (v) The Co(II), Ni(II), and Cu(II) ion complexes contained six, four, and two hydrated water molecules,

respectively. Their thermal degradation began at approximately 200, 175, and 150°C, respectively. This indicates that increased hydration correlates with greater thermal stability: the Co(II) complex, with six hydrated water molecules, was the most stable, while the Cu(II) complex, with two, was the least stable.

(vi) The thermal degradation of the synthesized metalligand complexes resulted in metal oxide compounds as the final products. The metal oxide compounds of CoO and CuO were contaminated with some residual carbon from the decomposition process, whereas the NiO contained no residual carbon from the decomposition process.

3.3 Biological evaluation

The antimicrobial activity of the free ligand and the synthesized complexes was evaluated against two Gramnegative bacteria and three Gram-positive bacteria. The test strains included E. coli and P. aeruginosa for Gramnegative, as well as B. subtilis, S. aureus, and S. pneumoniae for Gram-positive. The Kirby-Bauer disc diffusion method was employed to determine the antimicrobial potency, and the inhibition zone diameters (mm/mg sample) for the free ligand and synthesized complexes against the five bacterial strains are presented in Table 4. The free ligand exhibited relatively low antimicrobial activity, as evidenced by the inhibition zones of 8.0, 10.0, 10.0, 9.0, and 8.0 mm observed against E. coli, P. aeruginosa, B. subtilis, S. aureus, and S. pneumoniae, respectively. In contrast, the tetracycline antibiotic standard demonstrated significantly stronger inhibitory effects, with zone diameters of 32.0, 30.0, 35.0, 36.0, and 31.0 mm against the same bacterial species. This suggests the free ligand had relatively low antimicrobial potency compared to the tetracycline standard. The synthesized Co-L, Ni-L, and Cu-L complexes were also examined

against the five bacterial strains. Among the three complexes, the Cu-L complex exhibited the highest antimicrobial activity. The Cu-L complex demonstrated inhibition zones of 11.0, 15.0, 20.0, 17.0, and 18.0 mm against E. coli, P. aeruginosa, B. subtilis, S. aureus, and S. pneumoniae, respectively. Overall, the synthesized complexes displayed moderate antimicrobial activity against all of the tested bacterial strains. However, they exhibited enhanced antimicrobial potency in comparison to the free ligand. The findings suggest that the coordination of the metal ions with the synthesized ligand has augmented the antimicrobial properties of the ligand, with the Cu-L complex demonstrating the most promising activity.

The synthesized Co-L, Ni-L, and Cu-L complexes demonstrate superior antimicrobial activity compared to their corresponding free ligand, primarily due to structural alterations resulting from coordination. This chelation process converts the complexes into more effective bacteriostatic agents by impeding microorganism proliferation. This heightened antimicrobial efficacy supports both overtone's concept and chelation theory [23,24], which suggests that chelation enhances a ligand's ability to act as a bacterial agent. Chelation diminishes the polarity of the metal ions, bringing them into a more advantageous range. This decrease in polarity arises from the partial distribution of the metal ion's positive charge among donor groups and the overlapping of the ligand orbital, thereby improving the complexes' ability to permeate lipid membranes. By obstructing metal binding sites in microbial enzymes and improving the delocalization of π -electrons within the chelate ring, these complexes interfere with cell respiration, suppress protein synthesis, and limit the organism's capacity for growth. Consequently, metal complexes function as carriers for ligand activation, serving as the main cytotoxic agents, and generally exhibit greater activity than the ligands alone.

Several novel 1,3,5-triazine derivatives containing 4-amino-6-(tert-butyl)-3-(methylthio)-1,2,4-triazin-5(4H)-one and

Table 4: Inhibition zone diameters (mm/mg sample) of the free ligand and its complexes with Co(II), Ni(II), and Cu(II) ions against five bacterial strains

Sample	Inhibition zone diameter (mm/mg sample)					
	Gram-negative strains		Gram-positive strains			
	E. coli (G ⁻)	P. aeruginosa (G ⁻)	B. subtilis (G ⁺)	S. aureus (G ⁺)	S. pneumonia (G ⁺)	
Control: DMSO	0.0	0.0	0.0	0.0	0.0	
Standard: tetracycline	32.0	30.0	35.0	36.0	31.0	
Free ligand	8.0	10.0	10.0	8.0	9.0	
Co-L complex	10.0	11.0	16.0	13.0	15.0	
Ni-L complex	10.0	13.0	14.0	13.0	14.0	
Cu–L complex	11.0	15.0	20.0	17.0	18.0	

5-benzyl-1,3,4-thiadiazol-2-amine, as well as primary amines, were synthesized and evaluated for their in vitro antimicrobial properties against various Gram-positive and Gram-negative bacterial strains using a microdilution method. Numerous 1,3,5-triazine derivatives exhibited improved activity against two Gram-positive bacteria compared to the standard drug [25]. A new series of 1,2,4-triazine compounds bearing an indole group were synthesized and screened for their antimicrobial activity against E. coli, Proteus mirabilis, Staphylococcus epidermidis, and S. aureus using the disk diffusion method. Multiple derivatives in this series displayed excellent activity, surpassing the standard drug in terms of the zone of inhibition and minimum inhibitory concentration (MIC) [26]. Furthermore, several new 1,2,4-triazine derivatives were synthesized, and their antimicrobial activity was evaluated against four standard organisms, including the Gram-positive bacteria B. subtilis and S. aureus, as well as the Gram-negative bacterium Escherichia coli. 5-(4-Methoxybenzylidene)-6-chloro-2,5-dihydro-2,3-diphenyl-1,2,4-triazine and 8-(4-methoxybenzylidene)-5,8-dihydro-5,6-diphenyltetrazolo[1,5-f][1,2,4]triazine derivatives showed moderate activity against both the Grampositive B. subtilis and S. aureus. 4-(4-Methoxybenzylidene)-1,2-diphenyl-1H-[1,2,4]triazino[6,1-b]quinazolin-10(4H)-one derivative exhibited low activity only against S. aureus [27]. Additionally, a simple and efficient method for synthesizing 1,2,4-triazine derivatives, with the general formula 2-[4-(substituted-phenyl)-thiazol-2-yl]-5-(2-susbtituted quinolin-3-ylmethelene) 3-phenyl-2,5-dihydro-1H-[1,2,4]-triazine-6-one, was developed through the condensation of phenyl hydrazine and substituted 4-(2-chloro-quinoline-3yl methylene)-2-[phenyl-4H-oxazol-5-one in acetic acid solvent. Examination of the antimicrobial activities of the synthesized derivatives revealed moderate to good potency [28].

4 Conclusion

One of the 1,2,4-triazine derivatives was synthesized, and its metal complexes with Co(II), Ni(II), and Cu(II) ions were manufactured. The ligand, which is termed HL, was prepared from the reaction of 5-bromosalicylaldehyde and hippuric acid. The synthesized ligand was then used to capture the investigated metal ions. CHN and gravimetric analyses were employed to verify the complexation stoichiometry between the ligand and the metal ions. The created ligand-metal complexes were characterized using several spectroscopic techniques, and their thermal and microstructural properties were obtained and differentiated by thermogravimetric (DTG) measurements,

powder X-ray diffraction (XRD), and transmission electron microscopy (TEM). The results propose that the general compositions are [CoL(H2O)4]·Cl·6H2O for the ligand complex with Co(II), [NiL(H₂O)₄]·Cl·4H₂O for the ligand complex with Ni(II), and [CuL(H₂O)Cl]·2H₂O for the ligand complex with Cu(II). Furthermore, the changes in the morphology of the ligand's particles after coordination with the Co(II), Ni(II), and Cu(II) ions were examined, revealing that the originally rod-like particles transformed into a stone-like appearance, as shown by the TEM images. The antimicrobial activity of the synthesized complexes was evaluated against five microbial strains using the Kirby-Bauer disc diffusion method to determine how complexation affects the antimicrobial profile of the uncoordinated ligand. The complexes showed improved antimicrobial potency compared to the free ligand, although their activity was moderate against all tested bacterial strains. This indicates that coordination with metal ions substantially enhanced the ligand's antimicrobial characteristics, with the Cu(II) complex showing the most promising results. Future work will involve single-crystal X-ray diffraction, mass spectrometry (MS), and DFT-based modeling for more detailed characterization and interpretation of the synthesized metal complexes. Additionally, the biological investigation will be expanded to include cytotoxicity and DNAbinding properties of the synthesized complexes, aiming to comprehensively assess their pharmacological potential and provide a deeper understanding of their mechanism of action.

Acknowledgments: The authors extend their appreciation to Taif University, Saudi Arabia, for supporting this work through project number TU-DSPP-2024-59.

Funding information: This research was funded by Taif University, Saudi Arabia, Project No. TU-DSPP-2024-59.

Author contribution: The author confirms the sole responsibility for the conception of the study, presented results and manuscript preparation.

Conflict of interest: There is no conflict of interest associated with this manuscript.

Ethical approval: The conducted research is not related to either human or animals use.

Data availability statement: The datasets generated during and/or analyzed during the current study are available from the corresponding author on reasonable request.

References

- Alsawat M, Adam AMA, Refat MS, Alsuhaibani AM, El-Sayed MY. Structural, spectroscopic, and morphological characterizations of metal-based complexes derived from the reaction of 1-phenyl-2thiourea with Sr²⁺, Ba²⁺, Cr³⁺, and Fe³⁺ ions. Bull Chem Soc Ethiop. 2024:38:1803-14
- Adam AMA, Refat MS, Alsuhaibani AM, El-Saved MY, Preparation [2] and characterizations of metal-based complexes derived from the reaction of trizma base with Mg(II), Ca(II), and Ba(II) ions. Bull Chem Soc Ethiop. 2024;38:1791-801.
- Adam MSS. Synthetic and characteristic strategies of Fe^{II} and V^{IV}Ocomplexation from Schiff base diol chelating ligand for catalytic 1,2cyclooctene epoxidation and biological studies. I Mol Lig. 2025:426:127481
- Eichhorn GL, Marzilli LG. Advances in inorganic biochemistry models in inorganic chemistry. New Jersey: PTR Prentice-Hall, Inc; 1994.
- Hughes MN. The inorganic chemistry of biological processes. 2nd edn. Chichester, England: Wiley; 1984.
- [6] Alessio E. Bioinorganic medicinal chemistry. Germany: Wiley-VCH Verlag GmbH and Co. KGaA; 2011.
- Adam MSS, Alfurayj I, Alkhalifah MA, Al-Odail F, Abuelela AM, [7] Khalil A. Structural influence of new fabricated Co^{II} and Cu^{II}-diol Schiff-base complexes on catalytic epoxidizing reactions and biological efficacy. Res Chem Intermed. 2025;51:2243-85.
- Adam AMA, Refat MS, Gaber A, Grabchev I. Complexation of [8] alkaline earth metals Mg2+, Ca2+, Sr2+ and Ba2+ with adrenaline hormone: Synthesis, spectroscopic and antimicrobial analysis. Bull Chem Soc Ethiop. 2023;37:357-72.
- El-Sayed MY, Refat MS, Altalhi T, Eldaroti HH, Alam K. Preparation, [9] spectroscopic, thermal and molecular docking studies of covid-19 protease on the manganese(II), iron(III), chromium(III) and cobalt(II) creatinine complexes. Bull Chem Soc Ethiop. 2021:35:399-412.
- [10] Adam MSS, Bakhuraisa ZS, Abualreish MJA, Mohamad ADM, Mohamed MA. Manganese (II) complexes of thiophenyl iminoligand with synergistic behavior in biological systems, ct-DNA interactions, and catalytic oxidative performance of benzyl alcohol. Polyhedron. 2025;270:117441.
- [11] Adam MSS, Abualreish MJA, Mohamad ADM, Omran OA, Mohamed MA. Biological and catalytic evaluation for nickel (II) and oxyvanadium (II) chelates of tri-dentate hydrazone-quinoxalyl ligand. Appl Organomet Chem. 2025;39(3):e70057.
- [12] Alsuhaibani AM, Adam AMA, Refat MS. Four new tin(II), uranyl(II), vanadyl(II), and zirconyl(II) alloxan biomolecule complexes: synthesis, spectroscopic and thermal characterizations. Bull Chem Soc Ethiop. 2022;36:373-85.
- Mojos KD, Orvig C. Metallodrugs in medicinal inorganic chemistry. Chem Rev. 2014;114(8):4540-63.

- [14] Adam MSS, Makhlouf MM, Taha A, Khalil A, Mahmoud HA. Synergistic effect of copper(II) di-iminophenol complex catalyst immobilized on Fe₃O₄-TiO₂ nanocomposite: Homogeneity and heterogeneity in organic thiophene oxidation. J Taiwan Inst Chem Eng. 2025;168:105896.
- Guo ZH, Jin ZX, Wang JY, Pei J. A donor-acceptor-donor conjugated molecule: twist intramolecular charge transfer and piezochromic luminescent properties. Chem Commun. 2014;50:6088.
- [16] Saloutina LV, Zapevalov AY, Kodess MI, Slepukhin PA, Ganebnykh IN, Saloutin VI, et al. Trifluoromethyl-containing 1,2,4-triazines. Synthesis on the base of perfluorobiacetyl and reactions with thiosemicarbazide and thiourea. J Fluor Chem. 2019;227:109362.
- [17] Alroogi A, Al-Amshany ZM, Al-Harbi LM, Altalhi TA, Refat MS, Hassanien AM, et al. Spectroscopic and physicochemical studies on 1,2,4-triazine derivative. Coatings. 2022;12:714.
- Bauer AW. Antibiotic susceptibility testing by a standardized single [18] disc method. Am J Clin Pathol. 1966;45:149-58.
- [19] Chang JC, Hsueh PR, Wu JJ, Ho SW, Hsieh WC, Luh KT. Antimicrobial susceptibility of flavobacteria as determined by agar dilution and disk diffusion methods. Antimicrob Agents Chemother. 1997;41:1301-6.
- Madonna JM, Luis O, Victor LP, Jose RR, Enuo C, John H. Correlation **[201** between E-test, disk diffusion, and microdilution methods for antifungal susceptibility testing of fluconazole and voriconazole. Antimicrob Agents Chemother. 2003;47:1647-51.
- [21] Bellamy LJ. The infrared spectra of complex molecules. London: Chapman & Hall; 1975.
- Deacon GB, Phillips RJ. Relationships between the carbon-oxygen [22] stretching frequencies of carboxylato complexes and the type of carboxylate coordination. Coord Chem Rev. 1980;33(3):227-50.
- [23] Emara AAA. Structural, spectral and biological studies of binuclear tetradentate metal complexes of N₃O Schiff base ligand synthesized from 4,6-diacetylresorcinol and diethylenetriamine. Spectrochim Acta A. 2010;77:117-25.
- Abou-Hussein AAA, Linert W. Synthesis, spectroscopic and biological activities studies of acyclic and macrocyclic mono and binuclear metal complexes containing a hard-soft Schiff base. Spectrochim Acta A. 2012;95:596-609.
- Malik GM, Patel TV. Synthesis and study of 1,2,4-triazine and [25] thiadiazoles based derivatives of S-triazine as antimicrobial agents. I Asian Sci Res. 2017:7(6):214-23.
- [26] Arshad M, Bhat AR, Hoi KK, Choi I, Athar F. Synthesis, characterization and antibacterial screening of some novel 1,2,4triazine derivative. Chin Chem Lett. 2017;28:1559-65.
- Hashem HE, Abo-Bakr AM. Synthesis of some new 1,2,4-triazine and 1,2,5-oxadiazine derivatives with antimicrobial activity. Heteroat Chem. 2019;2019(1):2326514.
- Dawane BS, Kadam SN, Shaikh BM. An efficient synthesis of 1, 2, 4-[28] triazine derivatives and their in vitro antimicrobial activity. Der Pharmacia Lett. 2010;2(4):126-31.